Microchemical Journal 159 (2020) 105538

Contents lists available at ScienceDirect

Microchemical Journal

journal homepage: www.elsevier.com/locate/microc

Nickel oxide nanoparticles-modified glassy carbon electrodes for non-enzymatic determination of total sugars in commercial beverages

Iñigo Fernández [a], José Luis González-Mora [a], Pablo Lorenzo-Luis [b], Reynaldo Villalonga [c], Pedro A. Salazar-Carballo [a,*]

[a] Laboratory of Sensors, Biosensors and Advanced Materials, Faculty of Health Sciences, University of La Laguna, Campus de Ofra s/n, 38071 La Laguna, Tenerife, Spain
[b] Inorganic Chemistry Area, Section of Chemistry Faculty of Science; Instituto Universitario de Bio-Orgánica "Antonio González", University of La Laguna, Tenerife, Spain
[c] Department of Analytical Chemistry, Faculty of Chemistry, Complutense University of Madrid, 28040 Madrid, Spain

ARTICLE INFO

Keywords:
Nickel oxide nanoparticles
Non-enzymatic electrochemical sensor
Sugars
Afro-food industry

ABSTRACT

Nickel oxide nanoparticles of about 6 nm were obtained in two simple steps. Nanoparticles were characterized by using FTIR spectroscopy, TEM images, thermal analysis, X-ray diffraction and electrochemical techniques. GCEs were modified with nanoparticles by the casting method and their sensing properties were optimized. Electrochemical tests confirmed their excellent electrocatalytic properties, which are able to detect glucose, fructose, lactose and sucrose. Under optimized conditions NiO NPs-modified sensors showed a good sensitivity of about 3.06 A M^{-1} cm^{-2} (R^2:0.999), linear range up to 0.6 mM, a fast time response (ca. 3 s) with a limit of detection of 0.39 μM. Their selectivity was tested for common interferences with promising results. The application of the sensor in real samples was evaluated by determining the total sugar content in different commercial beverages with recoveries of about 100%.

1. Introduction

The detection of sugars in the agro-food industry and biological samples (e.g., blood, saliva…) has been one of the hot topics during the last decades. Sugars or carbohydrates are the main source of energy in the organism, but their high intake can cause diseases such as diabetes mellitus, obesity and cardio-vascular accidents that have become one of the major health afflictions worldwide [1–3]. Therefore, it is essential to have a precise control of the sugar content in food and beverages [4,5]. Nutritional control, the high and increasing rates of obesity and diabetes mellitus have created the need for new user-friendly analytical systems with better sensitivity and selectivity [3], low response times, and more importantly, at a low cost. Common methods for sugar detection such as differential refractometry, photometry, evaporative light-scattering detection (ELSD) are well reported in the literature. In addition, the determination of sugars using different chromatography techniques (e.g., high-performance liquid chromatography, supercritical fluid chromatography, thin-layer chromatography and ion chromatography) are commonly used in agro-food laboratories [6–11]. However, more efficient and user-friendly systems for sugar detection with low interference, high sensitivity and without the use of complex derivatization reagents and high cost instrumentation are still sought after. In this regard the electrochemical approach (amperometric biosensors and sensors) offers high analytical performance [12–16], with an adequate operational range, cheap and user friendly instrumentation and the possibility to obtain real-time measurements in the laboratory and/or on the production line for quality control processes in industrial applications [12–14,16–24].

Although, different electrochemical biosensors have been reported in the literature for glucose, fructose and lactose detection [25–29], they still present some drawbacks due to the biological nature of the enzymes such as low thermal, temporal and pH stability. In this regard, amperometry non-enzymatic sensors have been reported as an alternative with excellent results, overcoming the difficulties found in the biosensor approach. The use of different precious metals as well as non-precious metals and their oxides as sensing materials have been used during the last two decades and the results have demonstrated their effectiveness for glucose detection [3–5,11,30–34]. In addition, nanotechnology has allowed a great leap forward in all fields of research science, including sensor applications [35–38]. Nanomaterials have opened up a

* Corresponding author.
E-mail address: psalazar@ull.edu.es (P.A. Salazar-Carballo).

https://doi.org/10.1016/j.microc.2020.105538
Received 13 July 2020; Received in revised form 9 September 2020; Accepted 10 September 2020
Available online 13 September 2020

wide variety of applications (electronic, energy, remediation, medical and healthcare applications, etc.) thanks to their high capacity to be functionalized, high electrocatalytic properties, high ratio area/volume [39–43]. In addition, nanostructures (nanoparticles, nanopillars, graphene and carbon nanotubes derived materials) have been used in sensor and biosensor applications with excellent results [1,11,31,34,44–50]. Although different techniques have been used to obtain nanostructured oxide thin film-modified devices (Magnetron Sputtering, Physical Vapor Deposition, Chemical Vapor Deposition…) with the oblique angle approach [4,30,49], they need sophisticated infrastructure and high cost equipment. Therefore, wet chemical synthesis methods are still preferred due to their facilities and low cost of the starting materials [15,51].

Although noble metals and their metallic alloys have been reported for developing non-enzymatic glucose sensors, the high cost of such materials restricts their practical implementation. To solve this problem other more abundant materials such as non-precious transition metals have gained enormous attention in recent years. Among different possibilities, nickel is an excellent candidate due to its low cost, abundance, high catalytic activity for glucose oxidation in alkaline medium, high stability, and reproducibility of results. Therefore, nickel is the most intensively examined transition metal catalyst, in its different forms such as Ni, NiO, $Ni(OH)_2$ and Ni metal–organic complex [11].

The synthesis of high reactive NiO nanoparticles obtained in ethanol solution in two successive steps is described here: (1) precipitation of ($Ni(OH)_2$) precursor and (2) calcination of the precursor to obtain highly crystalline Bunsenite phase NiO NPs [52]. NiO NPs were then dispersed in water and deposited on the surface of Glassy Carbon electrodes (GCEs) to confirm the sensing properties of the NiO NPs. The electrocatalysis of the GCE/NiO electrode against common sugars used in agro-food applications (glucose, fructose, lactose, sucrose) was evaluated by cyclic voltammetry and constant potential amperometry with excellent catalytic activity for all sugars tested. In contrast with previous sensors reported in the literature, the sensor here was able to detect all sugars tested with excellent analytical properties (not only glucose). Finally, a GCE/NiO electrode was used to determine the total sugar concentration in common everyday beverages with excellent results, and was found to be a user-friendly method with excellent anti-interference properties, without complex sample treatment (1:10 dilution).

2. Materials and methods

2.1. Materials

$Ni(NO_3)\cdot 6\ H_2O$, ethanol, NaOH pellet and interference species such as acetaminophen acid, ascorbic, uric acid, NaCl and KCl were purchased from Sigma-Aldrich (reagent grade) and used as received without further purification. Commercial fruit juices and soda drinks were obtained from local markets.

2.2. Nickel oxide nanoparticles synthesis

The fabrication method was adapted from [53] with some modifications. Briefly, 3 g $Ni(NO_3)\cdot 6\ H_2O$ was transferred into a 500 mL round bottom flask and dissolved in 150 mL ethanol to form a clear green colored solution. Independently, 1 g NaOH was dissolved into ethanol (200 mL) under agitation and heated at 60 °C for 15 min. Then, the latter solution was drop wise added into the nickel nitrate solution under stirring (800 rpm) at room temperature for 2 h. The green colored powder obtained was centrifuged at 10 000 g and washed three times with double distilled water to remove byproducts formed during the reaction, and washed two times with ethanol. After this, the precursor product, $Ni(OH)_2$ powder, was dried at 60 °C overnight. Finally, the precursor powder was calcined for 45 min at 350 °C leading to dark green colored NiO NPs.

2.3. Construction of the NiO-modified glassy carbon electrode

NiO NPs-modified electrode was assembled by the casting method. Firstly, 10 mg of NiO NPs were dispersed in double distilled water and sonicated for 1 h. GCEs (3 mm diameter) were polished with alumina slurry, rinsed with water, sonicated in water and ethanol (2 min each one) and dried with N_2 stream. Lastly, GCEs were casted with 10 μL of the dispersion described above and dried at room temperature overnight. Optimization of NiO NPs concentration and volume dispersion used during the casting step are described below.

2.4. Material characterization

X-ray diffraction patterns were recorded with a Philips Panalytical X'Pert powder diffractometer with CuK_α ($\lambda = 1.540$ Å) radiation in the 2θ range from 5° to 100°. Transmission electron microscopy images were obtained using a JEOL JEM-2000 FX microscope. FTIR spectra were recorded with a Varian 670-IR spectrophotometer in the range 400–4000 cm^{-1}.

2.5. Electrochemical methods characterization

Electrochemical measurements such as Constant Potential Amperometry (CPA) and Cyclic Voltammetry (CV) were performed with a PalmSens4 potentiostat and PSTrace5 software (PalmSens). Electrochemical measurements were obtained using an Ag/AgCl (3 M KCl) reference electrode and a Pt wire as counter electrode. Electrochemical tests were carried out in 0.1 M NaOH solution.

3. Results and discussions

3.1. NiO nanoparticle characterization

NiO nanoparticles were obtained as described previously. After the chemical synthesis of the precursor, the light green colored $Ni(OH)_2$ powder obtained was calcined, leading to a dark green colored powder, NiO NPs. The thermal analysis of $Ni(OH)_2$ was obtained (Fig. SM1, *for details see Supplementary Materials*) to study the formation of the NiO NPs. Fig. SM1 shows the TG and DSC curves obtained in the temperature range from ca. 25 °C to 500 °C. The first weight loss happened (ca. 55%) rapidly between 75 and 125 °C with an endothermic peak centered at 100 °C, and corresponding to desorption of the water used during the washing step. The second weight loss occurred slowly between 225 and 350 °C, with an endothermic peaks centered at ca. 260 °C, and corresponding to the thermal decomposition of $Ni(OH)_2$ according to $Ni(OH)_2 \rightarrow NiO + H_2O$. The corrected value (after removing the water contribution) revealed a weight loss of 19%, very close to the theoretical value of 19.4% obtained from the previous equation [54]. The slight mass change between 350 and 500 °C can be attributed to desorption of oxygen from the surface of the NiO NPs [55]. For further studies, the Ni $(OH)_2$ was heated at 350 °C for 30 min.

In order to confirm the correct synthesis of the NiO NPs, the experimental diffractogram of the NiO NPs was compared with a commercial XRD database. Fig. 1a shows characteristic diffraction lines at ca. 36.9°, 43.4°, 62.7°, 74.9°, 79.1° and 94.7° that were assigned to (111), (200), (220), (311), (222) and (400) planes of Bunsenite (NiO) (JCPDS Card no. 004-0835). The presence of broad Bragg's diffraction peaks confirmed the formation of very small NiO NPs. The full-width at half maximum (FWHM) of the (200) XRD line and the Debye-Scherrer equation was used to estimate the average crystallite size value. The result here, with a value of about ca. 5 nm confirmed the nanoscale dimensions of the NiO NPs obtained. No other characteristic peaks of Ni $(OH)_2$ were detected in the experimental diffractogram, corroborating the successful synthesis of pure NiO NPs.

FTIR spectrum for the synthesized NPS was obtained to confirm their nature and purity. Fig. 1b shows a broad band centered at 938 cm^{-1},

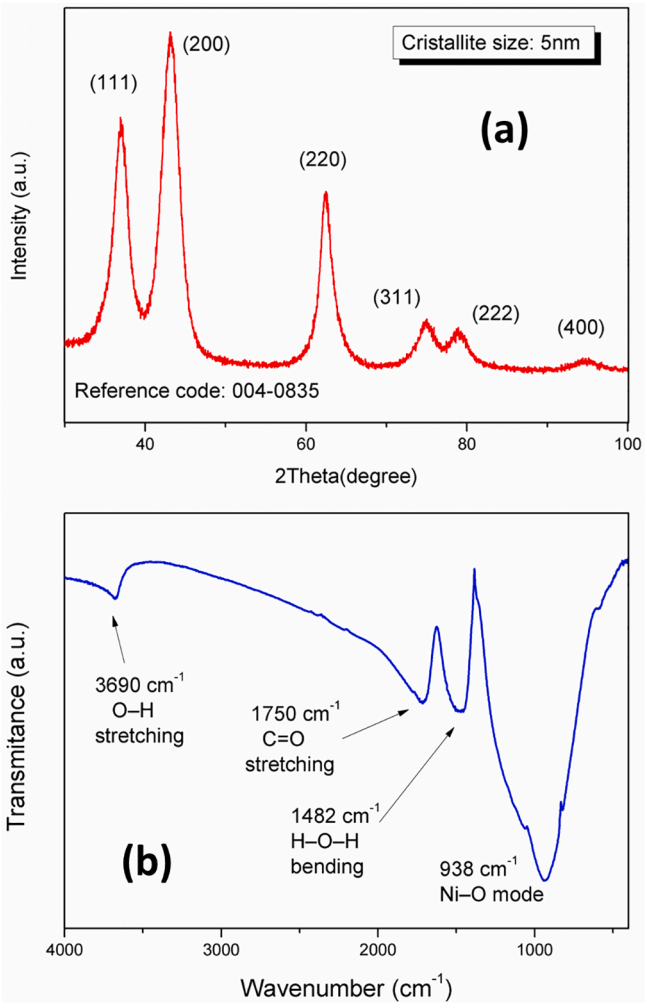

Fig. 1. Difractogram (a) and FTIR transmittance spectra (b) of nickel oxide nanoparticles.

which is attributed to the Ni-O mode of the Bunsenite NiO phase. Another two absorption bands related to bending and stretching modes of water molecules were observed at 1482 and 3691 cm^{-1}, respectively. Moreover, the last band (at ca. 1750 cm^{-1}, assigned to C = O stretching modes) confirmed the ability of the NPs to absorb both H_2O and CO_2 from the atmosphere during the sample preparation.

The structure and morphology of the synthesized NiO NPs was studied by transmission electron microscopy (TEM). Fig. 2a and b show the morphology of the NiO powder. The synthesized powder consisted of NPs with light agglomeration and with a certain degree of sharp edges. NiO NPs presented a normal size distribution (Fig. 2c) with a mean average particle size of 6.13 ± 2.87 (mean ± SD). Fig. 2d shows the selective area electron diffraction for the NiO powder and several well-defined diffraction rings associated to different crystalline planes are observed. Such an observation confirmed the initial XRD observation and corroborated that NiO NPs present certain degree of poly-crystallinity. Adjacent lattice fringes of the NiO NPs were calculated using the interplanar distance shown in Fig. 2e, presenting a value about 0.240 nm. Such a value corresponds to (1 1 1) planes of the Bunsenite NiO phase as reported above.

3.2. Electrochemical characterization

After sensor assembly and before their use for sugar detection, NiO NPs-modified GCEs (GCE/NiO) were cycled between 0 and 0.8 V (see Fig. 3a) in 0.1 M NaOH. The activation step produces stable oxide/hydroxide ($NiO/Ni(OH)_2$) species as reported previously in the literature [3,30,56,57]. The last step is indispensable for sugar detection because Ni(II)/Ni(III) compounds (e.g., $Ni(OH)_2$/NiOOH) act as catalytic redox intermediates in the electrochemical detection of sugars (e.g., glucose) [58–65] according to:

$$NiOOH + glucose + e^- \rightarrow glucolactone + Ni(OH)_2 \quad (1)$$

$$glucolactone \rightarrow gluconic\ \ acid(hydrolysi) \quad (2)$$

Fig. 3a shows the voltammograms recorded during the activation of the electrode. Two well-observed anodic (+0.4 V) and cathodic (+0.6 V) peaks appeared during this step, which are associated to Ni(0)/Ni(II)/Ni(III) redox reactions [64–66]. Therefore, NiO and $Ni(OH)_2$ species are generated at + 0.2 V according to [67]:

$$Ni + 2OH^- - 2e^- \leftrightarrow NiO + H_2O \quad (3)$$

$$Ni + 2OH^- - 2e^- \leftrightarrow Ni(OH)_2 \quad (4)$$

meanwhile, the Ni(II)/Ni(III) redox couple reaction occurs at a higher applied potential (+0.6 V), according to:

$$NiO + OH^- - e^- \leftrightarrow NiOOH \quad (5)$$

$$Ni(OH)_2 + OH^- \leftrightarrow NiOOH + H_2O + e^- \quad (6)$$

As observed in Fig. 3a the activation step produces an increase of both anodic and cathodic peak currents, increasing extraordinarily with each scan. Such behavior is accompanied by the shift of peak potentials. Such behavior has been ascribed to the surface enrichment in Ni(III) (β-$Ni(OH)_2$/ β-NiOOH species) and the ageing effect [3,30,56,58].

Fig. 3b shows the CVs recorded in 0.1 M NaOH for the unmodified GCE and the GCE/NiOs before and after activation. The unmodified-GCE electrode (inset) did not show any redox peak in the studied range of potential, only the current increase ascribed to the water splitting at potentials higher than ca. +0.7 V. Similar results were observed for the non-activated GCE/NiO electrode, the higher background current (capacitive contribution) observed can be explained by the larger electrode surface as a result of the NiO NPs deposited on it. The voltammogram for the activated GCE/NiO electrode presented a well-defined pair of peaks at about +0.6 and +0.4 V that is commonly attributed to Ni(II)/Ni(III) interconversion as reported above, and confirms the proper activation of the electrode for sensing applications.

The behavior of the cathodic and anodic peak currents against the scan rate was studied (Fig. 4a) by cycling the GCE/NiO electrode in 0.1 M NaOH solution in the range of scan rate between 5 and 150 mV s^{-1}. The results displayed a linear relationship between cathodic and anodic peak currents and the square of the scan rate (inset), suggesting that the reaction rate is limited by diffusion of reactants. As observed in Fig. 4a, the peak-to-peak separation potential increases with the scan rate. The latter behavior is characteristic for quasi-reversible systems where charge transfer processes limit the overall reaction rate [68]. Assuming that the reaction rate is completely restricted by charge transfer kinetic controlled by surface processes, and using the Laviron equation, the electron-transfer coefficient (α) and the apparent electron-transfer rate constant (k_s) values for the GCE/NiO electrode were determined according to previous works [69]. Therefore, the calculated values of the k_s and α for GCE/NiO electrode were about 0.15 s^{-1} and 0.79, respectively. The k_s value obtained was higher than previous values reported for NiO-modified ITO electrodes [49]. On the other hand, both ks and α values obtained were in good concordance with previously reported Ni-based GCEs [70].

The evaluation of the interface properties during the sensor assemble and its activation in alkaline conditions were evaluated with Electrochemical Impedance Spectroscopy (EIS) in ferri/ferro-cyanide ($[Fe(CN)_6]^{3-/4-}$) redox probe solution. Fig. SM2 shows the Nysquist curves for GCE (a) and NiO-modified GCE before (b) and after (c) its activation in 0.1 NaOH solution (potential limits = 0–0.9 V, scan rate = 0.1 V/s, n

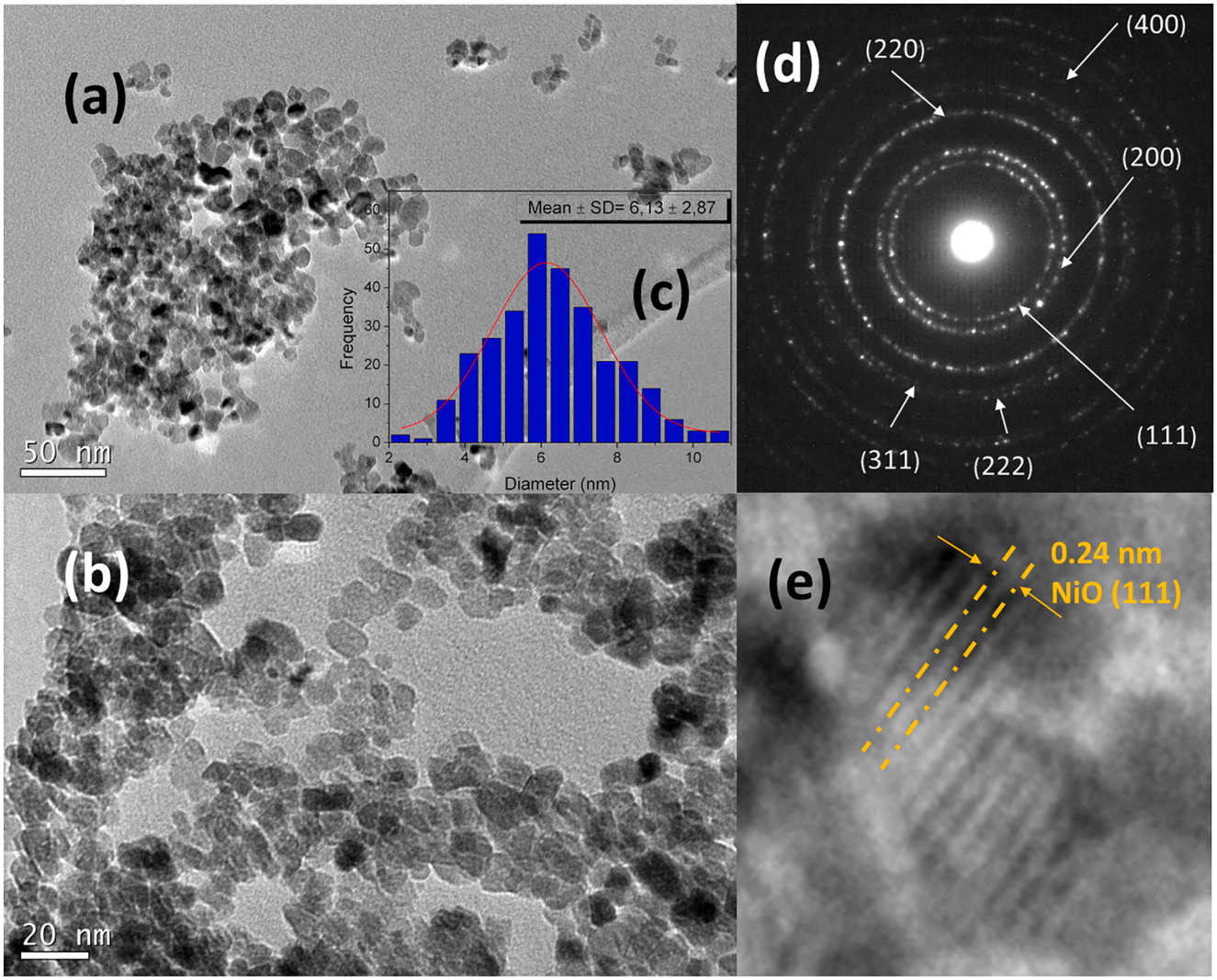

Fig. 2. SEM images for NiO NPs at different magnifications (a, b); size distribution of the NiO NPs (c); Selected Area Electron Diffraction pattern (SAED) acquired for NiO NPs; TEM image showing the NiO (1 1 1) d spacing (d).

= 30 cycles). The charge transfer resistance (R_{ct}) values of bare GCE and GCE/NiO before and after the activation step were calculated form Nysquist curves and found to be 8715, 38 and 176 Ω respectively. The justification for the decreasing of the R_{ct} value in the GCE/NiO configuration against the non-modified GCE can be justified due to electrostatic interaction of positively-charged NiO with negatively-charged redox probe solution (isoelectric point (NiO) = 9–11). The next increasing (after activation in alkaline solution) shows that the redox probe was repelled by negatively charged residual groups generated during the over-oxidation of the surface electrode in 0.1 M NaOH solution. Last finding results of vital importance due to in alkaline conditions the negatively-charged surface presents excellent anti-interference properties against most common interferences such as ascorbic and uric acid.

Fig. 4b shows the voltammograms recorded for the GCE/NiO electrode before and after adding glucose in the electrolyte solution. The CV without glucose displayed a pair of anodic and cathodic peaks centered at ca. +0.4 and +0.6 V and ascribed to the oxidation/reduction reactions of Ni(II)/Ni(III) species. The addition of glucose in the electrolyte solution (Fig. 4b) produced an increase in the anodic peak current ascribed to the increase of Ni(II) species (according Eq. (1)) and a slight shift to higher potentials. The latter observation can be attributed to restrictions imposed due to the absorption of glucose and/or intermediate and diffusion difficulties of glucose in the diffusion layer, contributing to decreasing the kinetics of the global reaction and producing the positive shift in the anodic current. In addition, Fig. 4b shows that the cathodic peak decreased slightly after glucose addition without any voltage shift, proving the excellent electrocatalytic properties of the GCE/NiO electrode and the non-reversibility of the glucose oxidation. Furthermore, the decrease in the cathodic current can be understood with Eq. (1), where the increment of glucose produces a depletion of Ni(III) species, hence producing a depletion of the cathodic current on the reverse scan. Such observations confirm that Ni(II)/Ni(III) species acts as a catalyst for the adequate oxidation of glucose to glucolactone.

3.3. Optimization of the main experimental variables

In order to optimize the sensor response, using glucose as the target analyte, the main experimental variables such as applied potential, electrochemical activation, NaOH concentration in the electrolyte solution, stirring rate during the analyte addition, nanoparticle concentration of the casting solution and volume deposited on the GCE during sensor assembly were studied step by step. In order to do this, sensor sensitivities, in the range from 0 to 1.5 mM, were obtained sequentially according to the order described above. For details see supporting information (Fig SM3 and Table SM1). The three first studied variables:

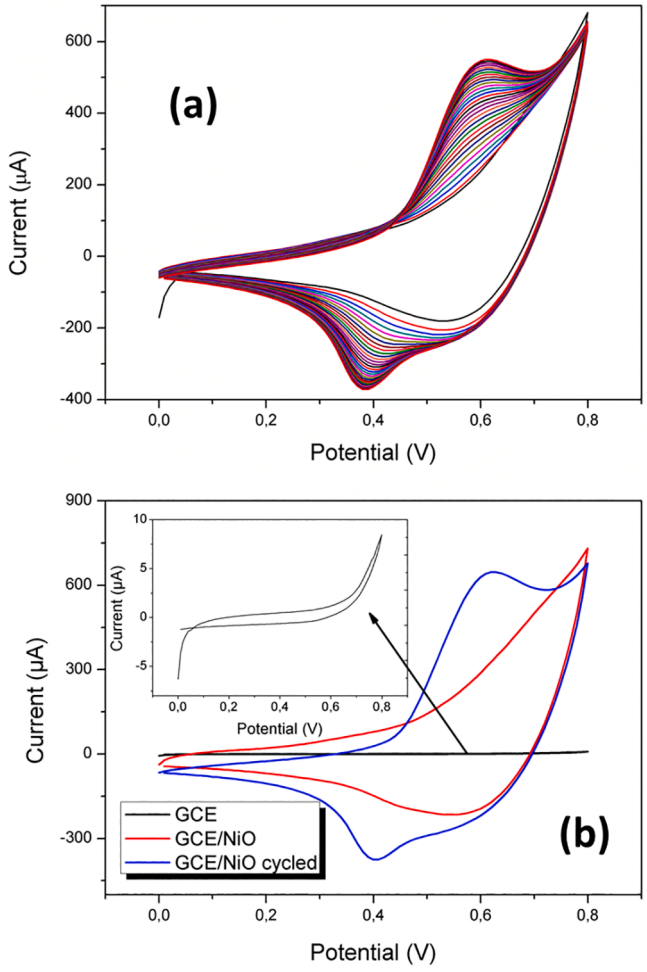

Fig. 3. (a) Electrochemical activation of the NiO NPs-modified electrode in 0.1 M NaOH electrolyte solution at 0.1 V s^{-1}. (b) cyclic voltamogram for Glassy Carbon Electrode (GCE, inset), non-activated (GCE/NiO) and activated (GCE/NiO cycled) NiO NPs-modified electrode in 0.1 M NaOH electrolyte solution at 0.1 V s^{-1}.

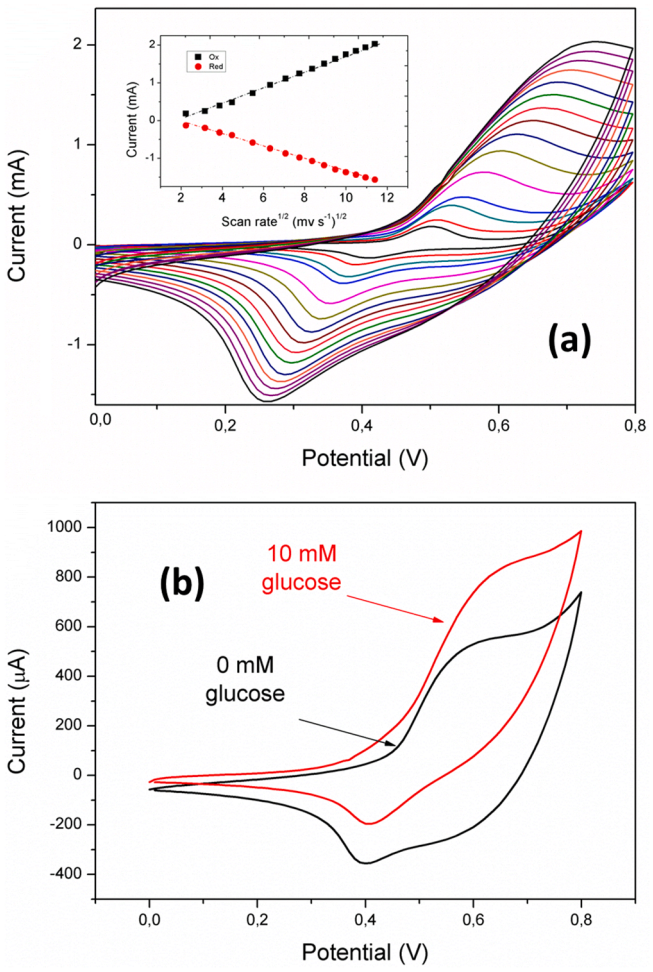

Fig. 4. (a) Cyclic voltammograms of the NiO NPs-modified electrode in 0.1 M NaOH electrolyte solution at different scan rates, inset: linear dependence of the anodic and cathodic peaks against the square root of the scan rate; (b) cyclic voltammograms of the NiO nanoparticle-modified electrode in 0.1 M NaOH electrolyte solution with and without 10 mM glucose at 0.05 V s^{-1}.

applied potential, number of activation cycles and NaOH concentration are related to the formation of active $Ni(OH)_2$/NiOOH species on the nanoparticle surface according to Eqs. (5) and (6) and the correct interconversion between Ni^{2+}/Ni^{3+} especies during the electrocatalytic oxidation of the analyte. The optimal working potential was found at 0.6 V, at higher potentials the sensitivity and stability of the sensor drastically decreased due to the higher background current, and the oxygen evolution ascribed to the water splitting. Such potential agree with the CV data reported above. The increase in the number of cycles during the activation step showed that 30 cycles were enough to improve the analytical performance of the sensor due to the generation of oxi/hydroxy species. The current response of the sensor under different alkaline conditions increased up to 0.1 M NaOH. Therefore, such NaOH concentration seems enough to get a high surface density of oxi/hydroxy species to improve the analytical performance of our sensor. As described above, the reaction rate on the sensor surface was limited by the diffusion of reactants. Therefore, the stirring rate of the solution during the calibration was conveniently evaluated. Our results concluded that a stirring rate of 1000 rpm is enough to ensure the appropriate supply of analyte to the sensor surface. Finally, the last two tested parameters are related to the nanoparticle loading on the electrode surface (nanoparticle concentration and volume of the casting solution). The optimal values for the nanoparticle concentration in the casting solution and the volume of the casting solution deposited on the electrode surface were 15 mg mL^{-1} and 20 μL respectively. Once such values were optimized, the increment of the amount of the nanoparticles deposited on the electrode surface produced a decrease of the analytical performance of the sensor that can be ascribed to the increase in the electron transfer resistance for large Ni nanoparticle loadings on the sensor surface.

3.4. Electrochemical determination of different sugars

The electrocatalytic properties of the GCE/NiO electrode against other common sugars found in agro-food samples were investigated using cyclic voltammetry. Fig. 5 shows the sensor response against different sugars (glucose, fructose, sucrose and lactose) before and after the addition of sugars in 0.1 M NaOH supporting electrolyte. All CVs showed a similar behavior, with a clear increase in the anodic peak (ascribed to the Ni(II)/Ni(III) redox center) and a slight shift to a higher potential as described above. These results confirmed the excellent electrocatalityc properties of the NiO NPs that are able to catalyze the adequate oxidation of different sugars. Based on the CV shape and the oxidation peak current, the results suggest that the catalytic activity of the GCE/NiO electrode is fairly similar for all the sugars tested. These findings are interesting due to the fact that common non-enzymatic electrochemical sensors reported in the literature can only detect glucose, and cannot be used for the determination of the total sugar

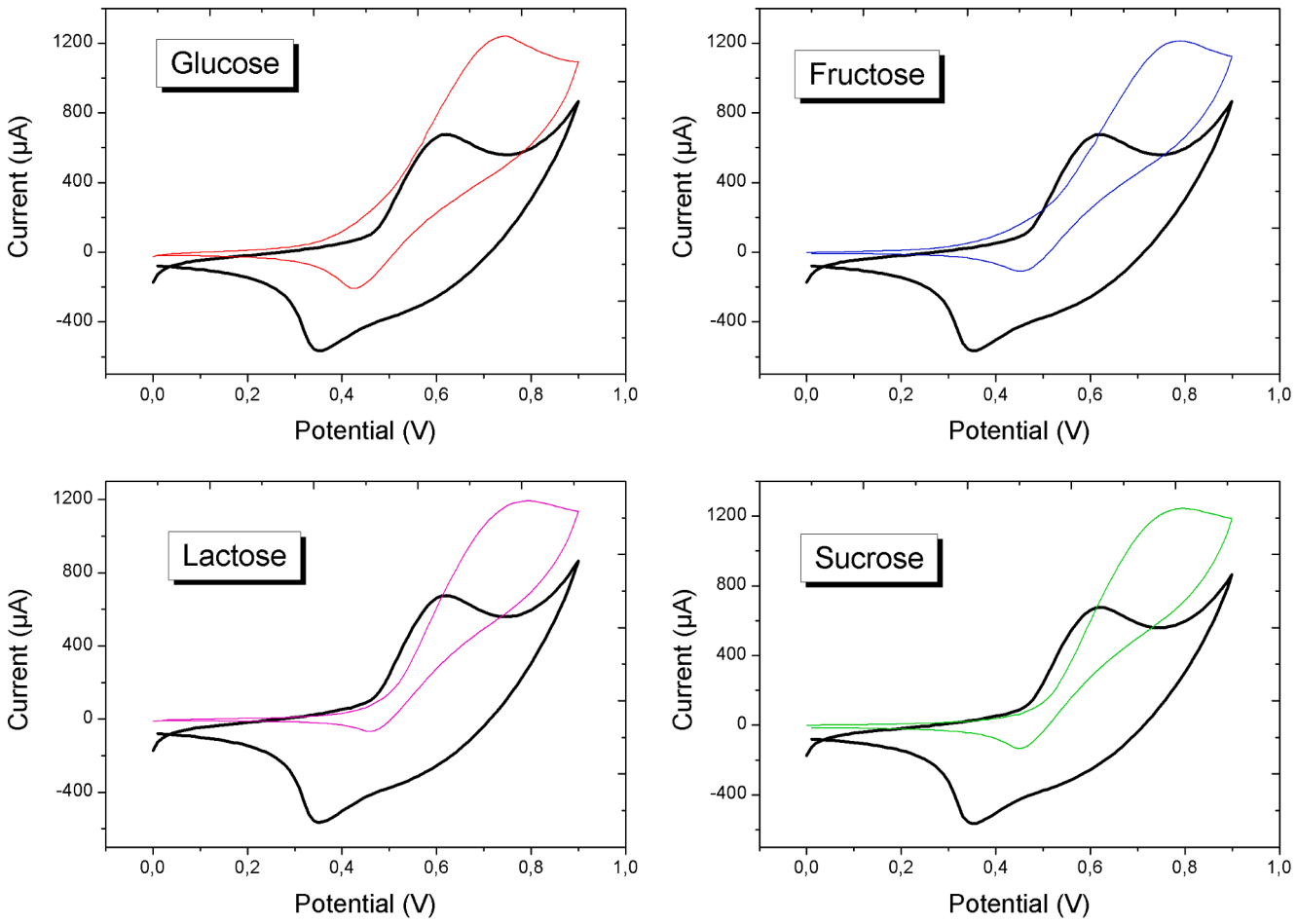

Fig. 5. Cyclic voltammograms of the NiO nanoparticle-modified electrode in 0.1 M NaOH electrolyte solution with and without 10 mM concentration of different sugars at 0.1 V s^{-1}.

concentration in agro-food samples. Therefore, such an approach offers the opportunity to develop an easy analytical detector for the fast and adequate determination of the total sugar concentration in agro-food applications, where glucose, fructose, lactose and sucrose are the most common sugars found in such matrixes [71,72].

In order to quantify the later observation above, a CPA technique was used to determine the sensitivity for each individual analyte under stirring conditions. Fig. SM4 shows the calibration curves for different sugars in a concentration range from 0 to 1.5 mM. An analysis in the linear region (until 600 μM, see Fig. 6a) confirmed that the sensitivities for all sugars are fairly similar.

Calibration parameters, summarized in Table 1, showed a high sensitivity for all the sugars with a mean value of 0.214 A M^{-1} (Fig. 6b), corresponding to a normalized sensitivity of about 3.06 ± 0.11 A M^{-1} cm^{-2} (mean ± SD, n = 4). This sensitivity value is higher than previous values reported in literature for glucose sensing [3,4,30,36,38,56,60–62,73–75].

Additionally, the sensor presented a time response ($t_{90\%}$) of about 3 s under stirring conditions for all sugars (for detail see Fig. SM5). The limit of detection, corresponding to a signal-to-noise of 3, for all sugars was ca. 0.39 μM. This behavior (higher sensitivity, fast time response and the ability to detect different sugars with similar sensitivity value) offer better analytical properties compared to non-enzymatic electrochemical sensors reported previously for agro-food application where one important quality control parameter of products is the total sugar content. In this regard, such a non-enzymatic sensor offers a simple and fast analytical method to determine the total sugar concentration compared with other more sophisticated techniques such as chromatography [10].

Moreover, the GCE/NiO electrode could be implemented in electrochemical detectors in HPLC chromatography devices to obtain a sugar profile for agro-alimentary samples.

Additional analyses were developed to study the reproducibility (using four different, but identically made sensors) and the repeatability (obtaining the sensitivity of the same electrode during four consecutive calibrations). The coefficient of variation obtained for such parameters were ca. 2.5 and 1.8% respectively, proving the excellent characteristics of the GCE/NiO electrode. NiO NPs stability stored in dry conditions at room temperature was evaluated over a period 3 months. In order to do this, different electrodes were assembled during this period without significant loss of signal, supporting the excellent stability of the NPs for analytical applications.

3.5. *Interference tests and total glucose determination in commercial beverages*

Interference tests were conducted in order to check the ability of the sensor to measure glucose and other sugars in real matrixes. In order to do this, the glucose amperometric current (I_{gluc}) of the GCE/NiO electrode was compared with the current of possible common interference substances (I_{int}) found in biological fluids and in commercial agro-food manufactured products. Fig. 7 shows the successive addition of 1 mM glucose and 0.1 mM for the selected interferences: NaCl, KCl, ascorbic acid (AA), citric acid (CA), uric acid (UA) and acetaminophen (AP). The results did not show significant responses for all interferences ($I_{int}/I_{gluc} \times 100 < 5\%$) and confirmed the excellent ability of the GCE/NiO electrode for analytical applications and quality control of agro-food and

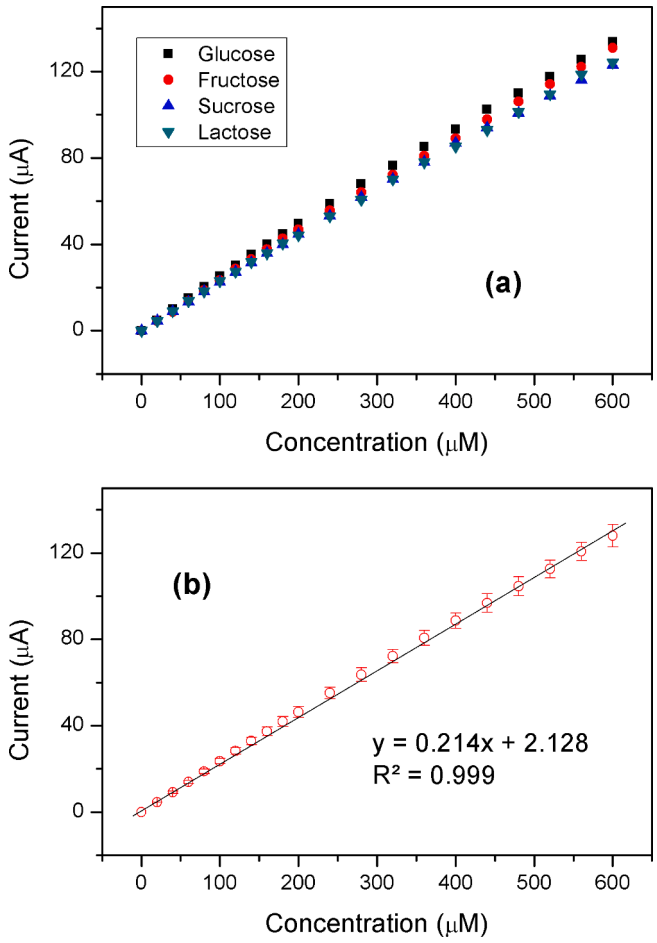

Fig. 6. (a) Calibration curves obtained for the GCE/NiO electrode in 0.1 M NaOH electrolyte solution for different sugars, applied potential: 0.6 V against Ag/AgCl (3 M) reference electrode; (b) Mean average calibration curve and linear fitting obtained with the data reported in (a).

Table 1
Sensitivities parameters for different sugars and the mean value for all sugars tested.

	Glucose	Fructose	Sucrose	Lactose	Sugars
Sensitivity (A M^{-1})	0.22	0.22	0.21	0.21	0.21
Sensitivity (A m^{-1} cm^{-2})	3.19	3.11	2.96	2.97	3.06
LOD (μM)	0.38	0.39	0.41	0.40	0.39
LOQ (μM)	1.25	1.28	1.35	1.35	1.31
LR (μM)	1.25–600	1.28–600	1.35–600	1.35–600	1.31–600
R-squared	0.998	0.999	0.998	0.999	0.999

LOD: limit of detection; LOQ: limit of quantification; LR: linear range.

manufactured products. Finally, the sensor was used for the quantitative sugar detection in soda drinks and commercial juices.

All checked samples were obtained from local markets and soda drinks were previously degassed (sonication for 10 min). Previous to sugar determination all samples were diluted in double distilled water (1:10) to adapt the concentration range of the sample to the linear range of the GCE/NiO electrode. For analytical purposes, glucose was selected as target analytical reference, since all sugars presented similar redox activity and sensitivity. Table 2 shows the total sugar concentration found and compared with the total sugar content labelled by the manufacturer. All data presented excellent recoveries and adequate coefficients of variation confirming the excellent properties of the

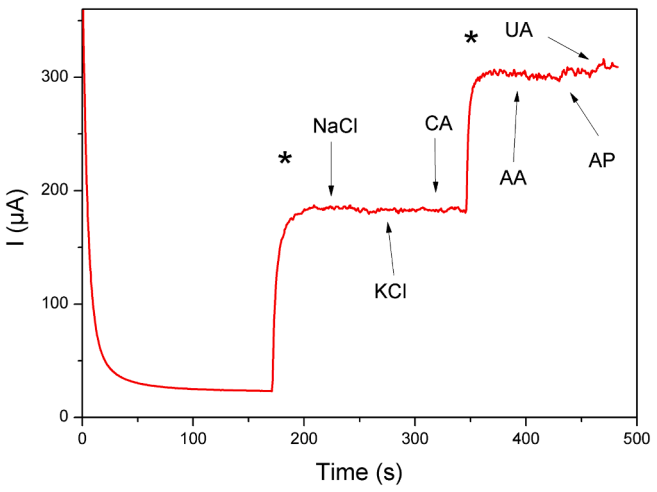

Fig. 7. (a) Amperometric response for the successive addition of 1 mM glucose and 0.1 mM for the selected interferences: NaCl, KCl, citric acid (CA), ascorbic acid (AA), uric acid (UA) and acetaminophen (AP), applied potential: 0.6 V against Ag/AgCl (3 M) reference electrode.

Table 2
Comparison of total sugars content in different commercial juices and beverages.

Sample	Certificated concentration (g/100 mL)	Total sugars (g/100 mL)	n	SD	CV %	Recovery (%)
Orange juice	4.2	4.0	3	0.3	8.0	96.0
Peach juice	4.2	4.4	3	0.4	8.2	104.8
Pear-Pineapple juice	13.6	13.7	3	0.2	1.5	100.7
Pear-Pineapple juice	11.5	11.1	3	0.2	1.4	96.8
Coke Soda	10.6	10.6	3	0.3	2.5	100.0
Coke Soda (Zero)	0	ND	3	–	–	–

ND: non-detected ($P < 0.05$).

reported sensor for use in agro-food applications. Comparing the data herewith previous data reported in the literature for commercial beverages and fruits juice samples, where sugar sensors can only measure glucose (and reporting recoveries close to 40–50%) [4,71,72], the sensor here presents a better analytical performance as it can detect different natural sugars, and such beverages are composed of glucose and other sugars such as fructose and/or sucrose in different proportions.

4. Conclusions

This work describes the synthesis and application of nickel oxide nanoparticles for the construction of a non-enzymatic sugar sensor. The difractogram confirmed that NiO nanoparticles presented excellent crystallinity, with a crystallite size of about 5 nm, corresponding with the Bunsenite NiO phase. The excellent electrocatalytic properties of this sensor allowed the detection of different sugars such as glucose, fructose, lactose and lactose which are of great interest in the agro-alimentary industry. Under optimized conditions NiO NPs-modified sensors showed a good sensitivity of about 3.06 A M^{-1} cm^{-2} (R^2:0.999), linear range up to 0.6 mM, a fast time response (ca. 3 s) with a limit of detection of 0.39 μM. The excellent recoveries obtained in commercial beverages showed the absence of matrix affect and interference in real samples.

Declaration of Competing Interest

The authors declare that they have no known competing financial interests or personal relationships that could have appeared to influence the work reported in this paper.

Acknowledgments

The authors would like to thank the SEGAI of the ULL for the XRD measurements.

Author statement

Iñigo Fernández and Pedro Salazar conceived of the presented study and developed the synthesis and the analytical measurements. Pablo Lorenzo-Luis and Reynaldo Villalonga helped in some characterization techniques and their interpretation. Pedro Salazar and José Luis González-Mora supervised the present study. All authors discussed the results and contributed to the final manuscript.

Appendix A. Supplementary data

Supplementary data to this article can be found online at https://doi.org/10.1016/j.microc.2020.105538.

References

[1] F. Arduini, L. Micheli, D. Moscone, G. Palleschi, S. Piermarini, F. Ricci, G. Volpe, Electrochemical biosensors based on nanomodified screen-printed electrodes: recent applications in clinical analysis, TrAC, Trends Anal. Chem. 79 (2016) 114–126.
[2] P. D'Orazio, Biosensors in clinical chemistry, Clin. Chim. Acta 334 (2003) 41–69.
[3] P. Salazar, V. Rico, R. Rodríguez-Amaro, J.P. Espinós, A.R. González-Elipe, New Copper wide range nanosensor electrode prepared by physical vapor deposition at oblique angles for the non-enzimatic determination of glucose, Electrochim. Acta 169 (2015) 195–201.
[4] P. Salazar, V. Rico, A.R. González-Elipe, Non-enzymatic glucose sensors based on nickel nanoporous thin films prepared by physical vapor deposition at oblique angles for beverage industry applications, J. Electrochem. Soc. 163 (2016) B704–B709.
[5] P. Salazar, V. Rico, A.R. González-Elipe, Nickel/copper bilayer-modified screen printed electrode for glucose determination in flow injection analysis, Electroanalysis 30 (2018) 187–193.
[6] H. Hinterwirth, M. Lämmerhofer, B. Preinerstorfer, A. Gargano, R. Reischl, W. Bicker, O. Trapp, L. Brecker, W. Lindner, Selectivity issues in targeted metabolomics: Separation of phosphorylated carbohydrate isomers by mixed-mode hydrophilic interaction/weak anion exchange chromatography, J. Sep. Sci. 33 (2010) 3273–3282.
[7] C. Antonio, T. Larson, A. Gilday, I. Graham, E. Bergström, J. Thomas-Oates, Quantification of sugars and sugar phosphates in Arabidopsis thaliana tissues using porous graphitic carbon liquid chromatography-electrospray ionization mass spectrometry, J. Chromatogr. A 1172 (2007) 170–178.
[8] S. Sawada, R. Ono, T. Sato, S. Suzuki, O. Arakawa, M. Kasai, Determination of sugar phosphates and nucleotides related to photosynthetic metabolism by high-performance anion-exchange liquid chromatography with fluorometric and ultraviolet detection, Anal. Biochem. 314 (2003) 63–69.
[9] D.B. Chu, K. Klavins, G. Koellensperger, S. Hann, Speciation analysis of sugar phosphates via anion exchange chromatography combined with inductively coupled plasma dynamic reaction cell mass spectrometry – optimization for the analysis of yeast cell extracts, J. Anal. At. Spectrom. 29 (2014) 915–925.
[10] N.M. Al-Mhanna, H. Huebner, R. Buchholz, Analysis of the sugar content in food products by using gas chromatography mass spectrometry and enzymatic methods, Foods 7 (2018) 185.
[11] D.-W. Hwang, S. Lee, M. Seo, T.D. Chung, Recent advances in electrochemical non-enzymatic glucose sensors – a review, Anal. Chim. Acta 1033 (2018) 1–34.
[12] H. Karimi-Maleh, F. Karimi, S. Malekmohammadi, N. Zakariae, R. Esmaeili, S. Rostamnia, M.L. Yola, N. Atar, S. Movaghgharnezhad, S. Rajendran, A. Razmjou, Y. Orooji, S. Agarwal, V.K. Gupta, An amplified voltammetric sensor based on platinum nanoparticle/polyoxometalate/two-dimensional hexagonal boron nitride nanosheets composite and ionic liquid for determination of N-hydroxysuccinimide in water samples, J. Mol. Liq. 310 (2020), 113185.
[13] H. Karimi-Maleh, K. Cellat, K. Arıkan, A. Savk, F. Karimi, F. Şen, Palladium-Nickel nanoparticles decorated on Functionalized-MWCNT for high precision non-enzymatic glucose sensing, Mater. Chem. Phys. 250 (2020), 123042.
[14] H. Karimi-Maleh, F. Karimi, M. Alizadeh, A.L. Sanati, Electrochemical sensors, a bright future in the fabrication of portable kits in analytical systems, Chem. Record 20 (2020) 682–692.
[15] H. Karimi-Maleh, O.A. Arotiba, Simultaneous determination of cholesterol, ascorbic acid and uric acid as three essential biological compounds at a carbon paste electrode modified with copper oxide decorated reduced graphene oxide nanocomposite and ionic liquid, J. Colloid Interface Sci. 560 (2020) 208–212.
[16] H. Karimi-Maleh, F. Karimi, Y. Orooji, G. Mansouri, A. Razmjou, A. Aygun, F. Sen, A new nickel-based co-crystal complex electrocatalyst amplified by NiO dope Pt nanostructure hybrid; a highly sensitive approach for determination of cysteamine in the presence of serotonin, Sci. Rep. 10 (2020) 11699.
[17] Y. Yi, M.N. Fiston, D. Zhang, G. Zhu, Nitrogen-doped carbon black/reduced graphene oxide nanohybrids for simultaneous electrochemical determination of hydroquinone and paracetamol, J. Electrochem. Soc. 167 (2020), 066510.
[18] M. Nodehi, M. Baghayeri, R. Ansari, H. Veisi, Electrochemical quantification of 17α – Ethinylestradiol in biological samples using a Au/Fe3O4@TA/MWNT/GCE sensor, Mater. Chem. Phys. 244 (2020), 122687.
[19] M. Baghayeri, M. Ghanei-Motlagh, R. Tayebee, M. Fayazi, F. Narenji, Application of graphene/zinc-based metal-organic framework nanocomposite for electrochemical sensing of As(III) in water resources, Anal. Chim. Acta 1099 (2020) 60–67.
[20] M. Rouhi, M.M. Lakouraj, M. Baghayeri, Low band gap conductive copolymer of thiophene with p-phenylenediamine and its magnetic nanocomposite: synthesis, characterization and biosensing activity, Polym. Compos. 40 (2019) 1034–1042.
[21] M. Ghanei-Motlagh, M.A. Taher, M. Fayazi, M. Baghayeri, A. Hosseinifar, Non-enzymatic amperometric sensing of hydrogen peroxide based on vanadium pentoxide nanostructures, J. Electrochem. Soc. 166 (2019) B367–B372.
[22] M. Baghayeri, R. Ansari, M. Nodehi, I. Razavipanah, H. Veisi, Label-free electrochemical bisphenol a aptasensor based on designing and fabrication of a magnetic gold nanocomposite, Electroanalysis 30 (2018) 2160–2166.
[23] M. Baghayeri, R. Ansari, M. Nodehi, H. Veisi, Designing and fabrication of a novel gold nanocomposite structure: application in electrochemical sensing of bisphenol A, Int. J. Environ. Anal. Chem. 98 (2018) 874–888.
[24] M. Baghayeri, R. Ansari, M. Nodehi, I. Razavipanah, H. Veisi, Voltammetric aptasensor for bisphenol A based on the use of a MWCNT/Fe3O4@gold nanocomposite, Microchim. Acta 185 (2018) 320.
[25] U.B. Trivedi, D. Lakshminarayana, I.L. Kothari, P.B. Patel, C.J. Panchal, Amperometric fructose biosensor based on fructose dehydrogenase enzyme, Sens. Actuators, B 136 (2009) 45–51.
[26] P. Bollella, Y. Hibino, K. Kano, L. Gorton, R. Antiochia, Highly sensitive membraneless fructose biosensor based on fructose dehydrogenase immobilized onto aryl thiol modified highly porous gold electrode: characterization and application in food samples, Anal. Chem. 90 (2018) 12131–12136.
[27] M. Ammam, J. Fransaer, Two-enzyme lactose biosensor based on β-galactosidase and glucose oxidase deposited by AC-electrophoresis: characteristics and performance for lactose determination in milk, Sens. Actuators, B 148 (2010) 583–589.
[28] M. Martín, A. González Orive, P. Lorenzo-Luis, A. Hernández Creus, J.L. González-Mora, P. Salazar, Quinone-Rich Poly(dopamine) Magnetic Nanoparticles for Biosensor Applications, ChemPhysChem, 15 (2014) 3742–3752.
[29] M. Martín, R.D. O'Neill, J.L. González-Mora, P. Salazar, The use of fluorocarbons to mitigate the oxygen dependence of glucose microbiosensors for neuroscience applications, J. Electrochem. Soc. 161 (2014) H689–H695.
[30] F.J. Garcia-Garcia, P. Salazar, F. Yubero, A.R. González-Elipe, Non-enzymatic Glucose electrochemical sensor made of porous NiO thin films prepared by reactive magnetron sputtering at oblique angles, Electrochim. Acta 201 (2016) 38–44.
[31] Z. Ji, Y. Wang, Q. Yu, X. Shen, N. Li, H. Ma, J. Yang, J. Wang, One-step thermal synthesis of nickel nanoparticles modified graphene sheets for enzymeless glucose detection, J Colloid Interface Sci 506 (2017) 678–684.
[32] J. Luo, S. Jiang, H. Zhang, J. Jiang, X. Liu, A novel non-enzymatic glucose sensor based on Cu nanoparticle modified graphene sheets electrode, Anal. Chim. Acta 709 (2012) 47–53.
[33] S. Viswanathan, T.N. Narayanan, K. Aran, K.D. Fink, J. Paredes, P.M. Ajayan, S. Filipek, P. Miszta, H.C. Tekin, F. Inci, U. Demirci, P. Li, K.I. Bolotin, D. Liepmann, V. Renugopalakrishanan, Graphene–protein field effect biosensors: glucose sensing, Mater. Today 18 (2015) 513–522.
[34] X. Zeng, Y. Zhang, X. Du, Y. Li, W. Tang, A highly sensitive glucose sensor based on a gold nanoparticles/polyaniline/multi-walled carbon nanotubes composite modified glassy carbon electrode, New J. Chem. 42 (2018) 11944–11953.
[35] F. Wang, Y. Feng, S. He, L. Wang, M. Guo, Y. Cao, Y. Wang, Y. Yu, Nickel nanoparticles-loaded three-dimensional porous magnetic graphene-like material for non-enzymatic glucose sensing, Microchem. J. 155 (2020), 104748.
[36] R. Fu, Y. Lu, Y. Ding, L. Li, Z. Ren, X. Si, Q. Wu, A novel non-enzymatic glucose electrochemical sensor based on CNF@Ni-Co layered double hydroxide modified glassy carbon electrode, Microchem. J. 150 (2019), 104106.
[37] L. Zhang, H. Liang, X. Ma, C. Ye, G. Zhao, A vertically aligned CuO nanosheet film prepared by electrochemical conversion on Cu-based metal-organic framework for non-enzymatic glucose sensors, Microchem. J. 146 (2019) 479–485.
[38] A. Mohamed Azharudeen, R. Karthiga, M. Rajarajan, A. Suganthi, Selective enhancement of non-enzymatic glucose sensor by used PVP modified on α-MoO3 nanomaterials, Microchem. J. 157 (2020), 105006.
[39] H. Karimi-Maleh, B.G. Kumar, S. Rajendran, J. Qin, S. Vadivel, D. Durgalakshmi, F. Gracia, M. Soto-Moscoso, Y. Orooji, F. Karimi, Tuning of metal oxides photocatalytic performance using Ag nanoparticles integration, J. Mol. Liq. 314 (2020), 113588.
[40] H. Karimi-Maleh, M. Shafieizadeh, M.A. Taher, F. Opoku, E.M. Kiarii, P. P. Govender, S. Ranjbari, M. Rezapour, Y. Orooji, The role of magnetite/graphene oxide nano-composite as a high-efficiency adsorbent for removal of

phenazopyridine residues from water samples, an experimental/theoretical investigation, J. Mol. Liq. 298 (2020), 112040.
[41] H. Karimi-Maleh, M. Sheikhshoaie, I. Sheikhshoaie, M. Ranjbar, J. Alizadeh, N. W. Maxakato, A. Abbaspourrad, A novel electrochemical epinine sensor using amplified CuO nanoparticles and a n-hexyl-3-methylimidazolium hexafluorophosphate electrode, New J. Chem. 43 (2019) 2362–2367.
[42] Z. Shamsadin-Azad, M.A. Taher, S. Cheraghi, H. Karimi-Maleh, A nanostructure voltammetric platform amplified with ionic liquid for determination of tert-butylhydroxyanisole in the presence kojic acid, J. Food Meas. Charact. 13 (2019) 1781–1787.
[43] F. Tahernejad-Javazmi, M. Shabani-Nooshabadi, H. Karimi-Maleh, Analysis of glutathione in the presence of acetaminophen and tyrosine via an amplified electrode with MgO/SWCNTs as a sensor in the hemolyzed erythrocyte, Talanta 176 (2018) 208–213.
[44] N. Abdul Halim, Y. Lee, R. Marugan, U. Hashim, Mediatorless impedance studies with titanium dioxide conjugated gold nanoparticles for hydrogen peroxide detection, Biosensors 7 (2017) 38.
[45] B. Borisova, A. Sánchez, S. Jiménez-Falcao, M. Martín, P. Salazar, C. Parrado, J. M. Pingarrón, R. Villalonga, Reduced graphene oxide-carboxymethylcellulose layered with platinum nanoparticles/PAMAM dendrimer/magnetic nanoparticles hybrids. Application to the preparation of enzyme electrochemical biosensors, Sensors Actuators B: Chemical 232 (2016) 84–90.
[46] A. Pandikumar, G.T. Soon How, T.P. See, F.S. Omar, S. Jayabal, K.Z. Kamali, N. Yusoff, A. Jamil, R. Ramaraj, S.A. John, H.N. Lim, N.M. Huang, Graphene and its nanocomposite material based electrochemical sensor platform for dopamine, RSC Adv. 4 (2014) 63296–63323.
[47] S. Rattana, N. Chaiyakun, N. Witit-anun, P. Nuntawong, S. Chindaudom, C. Oaew, P. Kedkeaw, Limsuwan, Preparation and characterization of graphene oxide nanosheets, Procedia Eng. 32 (2012) 759–764.
[48] P. Salazar, F.J. García-García, A.R. González-Elipe, Sensing and biosensing with screen printed electrodes modified with nanostructured nickel oxide thin films prepared by magnetron sputtering at oblique angles, Electrochem. Commun. 94 (2018) 5–8.
[49] P. Salazar, V. Rico, A.R. González-Elipe, Non-enzymatic hydrogen peroxide detection at NiO nanoporous thin film- electrodes prepared by physical vapor deposition at oblique angles, Electrochim. Acta 235 (2017) 534–542.
[50] R. Zhang, W. Chen, Recent advances in graphene-based nanomaterials for fabricating electrochemical hydrogen peroxide sensors, Biosens. Bioelectron. 89 (2017) 249–268.
[51] F. Tahernejad-Javazmi, M. Shabani-Nooshabadi, H. Karimi-Maleh, 3D reduced graphene oxide/FeNi3-ionic liquid nanocomposite modified sensor; an electrical synergic effect for development of tert-butylhydroquinone and folic acid sensor, Compos. B Eng. 172 (2019) 666–670.
[52] M. Miraki, H. Karimi-Maleh, M.A. Taher, S. Cheraghi, F. Karimi, S. Agarwal, V. K. Gupta, Voltammetric amplified platform based on ionic liquid/NiO nanocomposite for determination of benserazide and levodopa, J. Mol. Liq. 278 (2019) 672–676.
[53] M. Jamal, S. Chakrabarty, H. Shao, D. McNulty, M.A. Yousuf, H. Furukawa, A. Khosla, K.M. Razeeb, A non enzymatic glutamate sensor based on nickel oxide nanoparticle, Microsyst. Technol. 24 (2018) 4217–4223.
[54] J. Zhao, M. Yang, Z. Hua, Synthesis and magnetic properties of β-Ni(OH)2 and NiO nanosheets, J. Magn. Magn. Mater. 371 (2014) 10–13.
[55] C. Li, S. Liu, Preparation and characterization of Ni(OH)2 and NiO mesoporous nanosheets, J. Nanomater. 2012 (2012) 6.
[56] P. Salazar, V. Rico, A.R. González-Elipe, Nickel–copper bilayer nanoporous electrode prepared by physical vapor deposition at oblique angles for the non-enzymatic determination of glucose, Sens. Actuators, B 226 (2016) 436–443.
[57] K.E. Toghill, L. Xiao, M.A. Phillips, R.G. Compton, The non-enzymatic determination of glucose using an electrolytically fabricated nickel microparticle modified boron-doped diamond electrode or nickel foil electrode, Sens. Actuators, B 147 (2010) 642–652.
[58] C.R.G. Toghill K.E., Electrochemical non-enzymatic glucose sensors: a perspective and an evaluation. Int. J. Electrochem. Sci., 5 (2010) 1246-1301.
[59] J. Chen, J. Zheng, A highly sensitive non-enzymatic glucose sensor based on tremella-like Ni(OH)2 and Au nanohybrid films, J. Electroanal. Chem. 749 (2015) 83–88.
[60] W. Gao, W.W. Tjiu, J. Wei, T. Liu, Highly sensitive nonenzymatic glucose and H2O2 sensor based on Ni(OH)2/electroreduced graphene oxide−Multiwalled carbon nanotube film modified glass carbon electrode, Talanta 120 (2014) 484–490.
[61] M. Li, X. Bo, Z. Mu, Y. Zhang, L. Guo, Electrodeposition of nickel oxide and platinum nanoparticles on electrochemically reduced graphene oxide film as a nonenzymatic glucose sensor, Sens. Actuators, B 192 (2014) 261–268.
[62] Y. Liu, H. Teng, H. Hou, T. You, Nonenzymatic glucose sensor based on renewable electrospun Ni nanoparticle-loaded carbon nanofiber paste electrode, Biosens. Bioelectron. 24 (2009) 3329–3334.
[63] A. Sun, J. Zheng, Q. Sheng, A highly sensitive non-enzymatic glucose sensor based on nickel and multi-walled carbon nanotubes nanohybrid films fabricated by one-step co-electrodeposition in ionic liquids, Electrochim. Acta 65 (2012) 64–69.
[64] W.-D. Zhang, J. Chen, L.-C. Jiang, Y.-X. Yu, J.-Q. Zhang, A highly sensitive nonenzymatic glucose sensor based on NiO-modified multi-walled carbon nanotubes, Microchim. Acta 168 (2010) 259–265.
[65] Y. Zhang, Y. Wang, J. Jia, J. Wang, Nonenzymatic glucose sensor based on graphene oxide and electrospun NiO nanofibers, Sens. Actuators, B 171–172 (2012) 580–587.
[66] G.-F. Cai, J.-P. Tu, J. Zhang, Y.-J. Mai, Y. Lu, C.-D. Gu, X.-L. Wang, An efficient route to a porous NiO/reduced graphene oxide hybrid film with highly improved electrochromic properties, Nanoscale 4 (2012) 5724–5730.
[67] L.-M. Lu, L. Zhang, F.-L. Qu, H.-X. Lu, X.-B. Zhang, Z.-S. Wu, S.-Y. Huan, Q.-A. Wang, G.-L. Shen, R.-Q. Yu, A nano-Ni based ultrasensitive nonenzymatic electrochemical sensor for glucose: Enhancing sensitivity through a nanowire array strategy, Biosens. Bioelectron. 25 (2009) 218–223.
[68] E. Laviron, General expression of the linear potential sweep voltammogram in the case of diffusionless electrochemical systems, J. Electroanal. Chem. Interfacial Electrochem. 101 (1979) 19–28.
[69] P. Salazar, M. Martín, R.D. O'Neill, R. Roche, J.L. González-Mora, Surfactant-promoted Prussian Blue-modified carbon electrodes: enhancement of electro-deposition step, stabilization, electrochemical properties and application to lactate microbiosensors for the neurosciences, Colloids Surf., B 92 (2012) 180–189.
[70] A. Cardoso de Sá, L. Lataro Paim, N. Ramos Stradiotto, Sugars electrooxidation at glassy carbon electrode decorate with multi-walled carbon nanotubes with nickel oxy-hydroxide, Int. J. Electrochem. Sci. 9 (2014) 7746–7762.
[71] R.W. Walker, K.A. Dumke, M.I. Goran, Fructose content in popular beverages made with and without high-fructose corn syrup, Nutrition 30 (2014) 928–935.
[72] E.E. Ventura, J.N. Davis, M.I. Goran, Sugar content of popular sweetened beverages based on objective laboratory analysis: focus on fructose content, Obesity 19 (2011) 868–874.
[73] F. Cao, S. Guo, H. Ma, D. Shan, S. Yang, J. Gong, Nickel oxide microfibers immobilized onto electrode by electrospinning and calcination for nonenzymatic glucose sensor and effect of calcination temperature on the performance, Biosens. Bioelectron. 26 (2011) 2756–2760.
[74] Z. Amirzadeh, S. Javadpour, M.H. Shariat, R. Knibbe, Non-enzymatic glucose sensor based on copper oxide and multi-wall carbon nanotubes using PEDOT:PSS matrix, Synth. Met. 245 (2018) 160–166.
[75] J. Yang, M. Cho, C. Pang, Y. Lee, Highly sensitive non-enzymatic glucose sensor based on over-oxidized polypyrrole nanowires modified with Ni(OH)2 nanoflakes, Sens. Actuators, B 211 (2015) 93–101.